

# Tension Control in Roll-to-Roll Mechanical Peeling for 2D Material Transfer and Transfer Printing

Qishen Zhao<sup>1</sup>, Christopher Martin<sup>1</sup>, Nan Hong<sup>1</sup>, Dongmei Chen<sup>1</sup>, Wei Li<sup>1</sup>

<sup>1</sup> University of Texas at Austin, Department of Mechanical Engineering, Austin, TX, United States

## ABSTRACT

A major challenge of the large-scale application of two-dimensional (2D) materials is the scaling up of the process for its growth and transfer. Mechanical peeling has been demonstrated to be a promising method for transferring graphene in a fast and environmentally friendly manner. However, efforts in scaling up the process have been lacking. Performing mechanical peeling using a roll-to-roll (R2R) system could significantly increase the throughput of graphene transfer. Such a R2R process does not exist in industry. In this paper a novel R2R mechanical peeling system that has both speed and tension control capabilities is presented. Controllers that control the peeling tensions on both sides of the peeling front are developed based on a tension dynamics model. Both controllers contain a feedback and a feedforward term to account for large steady-state error. The control performance is validated using both experiments and simulation, demonstrating that the R2R mechanical peeling technique can be a viable method for dry transfer of 2D materials in a high-throughput industrial setting.

**Keywords:** roll-to-roll, 2D materials, dry transfer, tension control, zero phase error tracking

## NOMENCLATURE

$\omega_1$	unwinding roller speed
$u_2, u_3$	torque on rewinding roller
$v_1, v_2, v_3$	winding roller speed
$D_1, D_2, D_3$	roller distance
$A_2, A_3$	web cross sectional area
$h_{w2}, h_{w3}$	web thickness
$b$	web width
$E_2, E_3$	web stiffness
$\varepsilon_1, \varepsilon_2, \varepsilon_3$	web strain
$f_2, f_3$	friction coefficient
$J_2, J_3$	roller rotational inertia
$R, R_2, R_3$	idler and rewinding roller diameter

## 1. INTRODUCTION

Significant research effort has recently been devoted to developing R2R processes for production of flexible devices, because R2R production is superior to batch-style processes in a variety of ways. Primarily, R2R processes are

continuous, while batch style processes are discrete. This difference allows R2R processes to have a higher throughput than batch-style processes because the time wasted unloading and re-loading in batch-style processes can be eliminated. R2R processes that produce chemical vapor deposition (CVD) graphene [1,2], flexible electronics [3], and solar cells [4, 5] currently exist. The mechanical peeling process presented in this paper and in [6-9] proposes to take the next step: transferring these devices from their growth substrate onto a target substrate in a continuous, R2R manner. Thus, once the mechanical peeling process is fully developed and integrated with the mature R2R production technology, there will be a way to produce two-dimensional (2D) material-based devices and place them on a functional substrate in a high-throughput and continuous manner. Another benefit of the mechanical peeling method is that it is a dry transfer process, meaning it does not use any chemical etchants to move the device. This contrasts with typical transfer processes for CVD graphene, which are normally discrete and involve toxic etchants [6].

R2R dry transfer based on mechanical peeling was recently proposed and a testbed for large-scale graphene transfer was built [8, 10]. In this paper we develop a new R2R mechanical peeling system that enables simultaneous web speed and tension control. Web tension control is important in the R2R peeling process because it can be used to set the angle of the peeling front of the dry transfer process. For the transfer of CVD graphene, this angle is a critical control parameter [7]. Variation in the peeling angle can negatively affect the quality of the transferred material. Also, researchers have studied how different peeling angles affect the quality of the transferred 2D material [11]. Through analysis, an optimal peeling angle of 45° was found. For flexible electronics, all current transfer processes involve using stamps to transfer the device from its growth substrate to a target substrate. The current focus in this technological field is in finding different ways to vary the stamp adhesion energy between the pickup and deposition step of the transfer [12, 13]. A type of stamp that has the potential to be used in a R2R transfer process is the shear-assisted stamp [14]. The adhesion energy of these stamps varies with the retraction angle. It is possible to have a stamp pick up the flexible device at one angle and then deposit it at another angle. This process flow could be amenable to a R2R process where the angle of the transfer web changes between the pickup and drop-off locations. Thus, angle control is a critical component of the dry transfer processes for 2D materials such

as graphene and for future continuous transfer methods for flexible electronics.

Controlling the peeling angle of the R2R dry transfer process is challenging. The adhesion energy between the laminated webs is rarely stable, and the peeling angle is highly dependent on that parameter. Thus, precise and quick tension control is critical to quickly correct an error in the peeling angle due to disturbances. This paper presents a peeling tension control scheme. A feedback controller is designed based on a linear web tension dynamic model. To decrease the response time of the tension control, this paper also introduces a feedforward term based on the zero phase error tracking control (ZPETC) technique [15, 16]. This added term will enable the mechanical dry transfer system to respond quickly to errors in the peeling angle such that the quality of the device transfer can be maximized. Thus, the controller presented here has the potential to improve the viability of the R2R dry transfer of flexible materials and devices in a high-throughput industrial setting.

## 2. SYSTEM DESIGN AND INTEGRATION

The R2R mechanical peeling system is shown in Fig. 1. The modules are mounted on a 48-inch by 28-inch aluminum plate. The setup is secured on an optical breadboard.

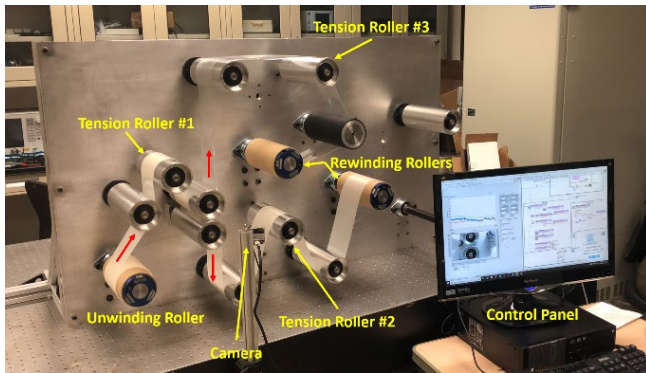


Figure 1: R2R system setup [7]

The laminate to be peeled is wound on a rewinding roller. The roller is actuated by a NEMA 23 (1-DM542S-23HS45) stepper motor. The use of stepper motor enables an open loop control of the speed with which the laminate is fed to the process. There are two rewinding rollers used to collect the separated thin films. The rewinding rollers are actuated by brushless servos (Aerotech BM130). The servo motors allow for torque control. Encoders are integrated with the motors so that the rewinding velocity can be measured. The idler rollers have ball bearings and the friction is low. In addition, the idler rollers have low rotational inertia and their effect on the process are negligible.

In the R2R peeling process, tension is an important factor affecting the peeling condition and therefore the quality of the obtained product. There are three tension zones in the R2R peeling system. In order to constantly monitor the tensions applied on the three tension zones, three load cells

(MAGPOWR CL-1-50) as in Fig. 2 are instrumented on idler rollers to measure the force applied. The idler rollers instrumented with load cells are the tension rollers in Fig. 1. The tension applied on the web can be calculated based on the load cell force reading and the geometry of the web path.



Figure 2: Load cell to measure web tension

A camera (Sony IMX291 Image Sensor) focusing on the peeling front location is installed to monitor the peeling process in real time. The images captured are used for system model validation and peeling analysis.



Figure 3: Peeling front geometry

The overview of the electronic system architecture is shown in Fig. 4. The R2R system is controlled by a NI CompactRIO 9022. The RT target is responsible for taking sensor measurements from the FPGA target and generating control signals to drive the winding motors. The FPGA target is responsible for interfacing with sensors and actuators. An analog output module (NI 9263) is used to generate torque command to the brushless servo drive. A digital IO module (NI 9404) is used to interface with encoders and stepper motor drive. An analog input module (NI 9205) is used to take tension measurements from the load cell amplifier. The CompactRIO communicates with a host PC through a GUI. The user interface allows the user to set desired process conditions such as peeling speed and tensions. The camera images are also shown in the GUI for peeling process monitoring.

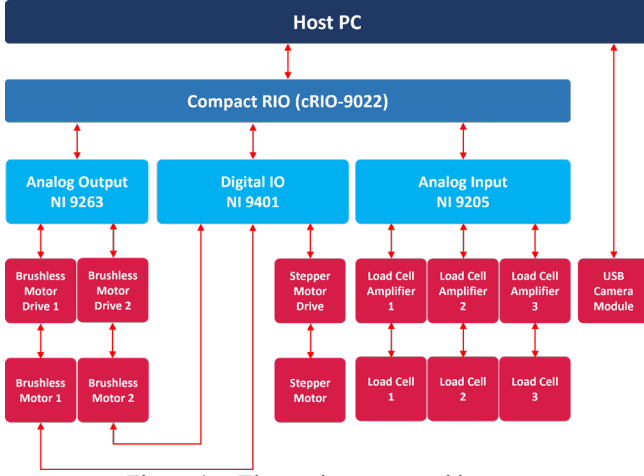


Figure 4: Electronic system architecture

### 3. MODELING AND CONTROL OF PEELING TENSIONS

#### 3.1 Peeling Model

A system model that captures the transient dynamics during the R2R peeling process was discussed in our previous result [17]. A schematic of the model is shown in Fig. 5. As shown in Fig.5 (a), The unwinding roller has an unwinding speed of  $\omega_1$  set by the user, resulting in an unwinding linear line speed of  $v_1$ . The rewinding rollers have linear speeds of  $v_2$  and  $v_3$ . The rewinding rollers are actuated by torque inputs  $u_2$  and  $v_3$ . The distances from the nipping rollers to the adjacent unwinding/rewinding rollers are  $D_1$ ,  $D_2$  and  $D_3$ . The total length of the web is  $D_i$  plus the colored line section. Before the peeling, the laminate is subject to tension  $t_1$ , and the peeled webs are subject to  $t_2$  and  $t_3$ , respectively. The peeling front geometry can be characterized with peeling angles  $\theta$  and  $\alpha$ . The peeling angle  $\theta$  can be further divided into  $\theta_1$  and  $\theta_2$  by the extension line of tension  $t_1$ , as shown in Fig.5 (b).

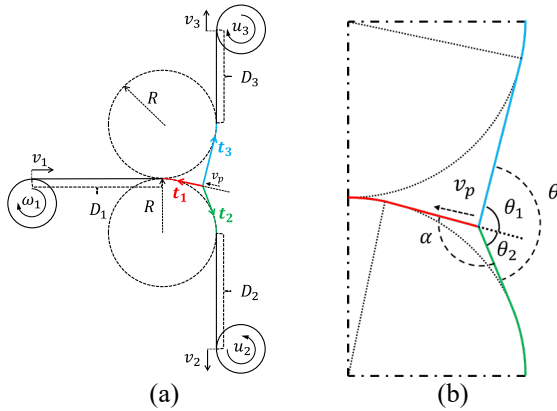


Figure 5: (a) R2R peeling system schematic [17], (b) peeling front

Based on our previous results, in the peeling process shown in this study, there always exists a force balance

formed by the three tensions on the three sides of the peeling front as [7]

$$t_2 + t_3 \cos \theta + t_1 \cos \alpha = 0 \quad (1)$$

$$t_1 \sin \alpha = t_3 \sin \theta \quad (2)$$

where

$$\theta = \theta_1 + \theta_2 \quad (3)$$

$$\alpha = \pi - \theta_2. \quad (4)$$

Additionally, the peeling process is feasible when the following condition is met:

$$G = \Gamma(v_p) \quad (5)$$

$$G = \frac{t_3}{b} (1 - \cos \theta_1 + \varepsilon_3 - \varepsilon_1 \cdot \cos \theta_1) + \frac{t_2}{b} (1 - \cos \theta_2 + \varepsilon_2 - \varepsilon_1 \cdot \cos \theta_2) - \frac{h_{w3} \cdot E_3}{2} (\varepsilon_3^2 - \varepsilon_1^2) - \frac{h_{w2} \cdot E_2}{2} (\varepsilon_2^2 - \varepsilon_1^2) \quad (6)$$

where  $G$  is the energy release rate and  $\Gamma$  is the adhesion energy between the two thin films  $G$  is a function of tensions. Peeling will happen if Eqn. (5) is satisfied. If the instantaneous  $G$  is less than the adhesion energy, peeling will not happen.

A steady state analysis is performed to show the effect of changing tensions on the resulting steady state peeling front condition. The analysis simulates a peeling process at a constant web speed, with the effective fracture energy  $\Gamma$  being a constant of 157 N/m. The Young's modulus of the material is considered to be 2.7 GPa, and the web width is 4 inch. The thicknesses of the upper and lower webs are 254  $\mu\text{m}$  and 127  $\mu\text{m}$ , respectively. The feasible peeling tension combinations that allows peeling to happen is shown in Fig. 6. Peeling is only feasible when the peeling tensions  $t_2$  and  $t_3$  fall into the highlighted region. The effect of changing  $t_2$ ,  $t_3$  on angle  $\theta$  and  $\alpha$  are shown in Fig. 7(a) and (b) respectively. Here, the peeling tensions are set as  $t_2 = 10$  N and  $t_3 = 15$  N. Based on the graphs in Fig. 7, it can be seen that a condition  $\theta$  of 144.12° and  $\alpha$  of 76.23° can ensure the peeling front to propagate steadily. The condition is highlighted by the red dot in the figure. The peeling tensions are then changed to  $t_2 = 15$  N and  $t_3 = 20$  N, and the equilibrium peeling angles shift to  $\theta = 115.90^\circ$  and  $\alpha = 109.20^\circ$ , which are highlighted by the blue dot in the figure.

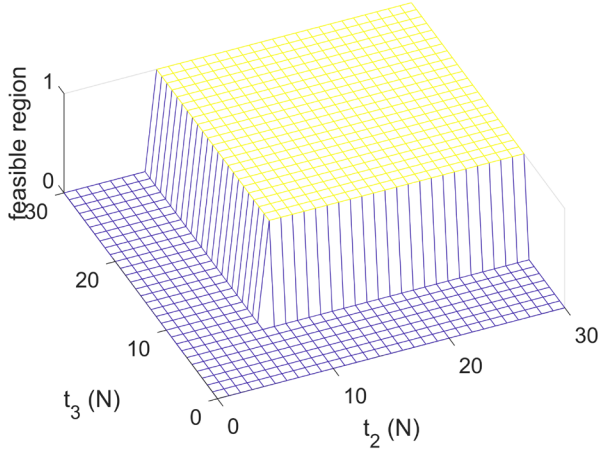


Figure 6: Feasible peeling tension region

The above analysis shows that in order to maintain a constant peeling condition when the adhesion energy is a constant, peeling tensions need to be maintained. For peeling tension control, a tension dynamic model for a single peeling arm is considered. The web between the peeling front and the rewinding roller can be approximately modeled as an elastic spring with a stiffness of  $K_i = \frac{A_i E_i}{D_i}$ . The tension dynamics can be written as

$$\dot{t}_i = K_i \cdot (v_i - v_1), \quad i = 2, 3 \quad (7)$$

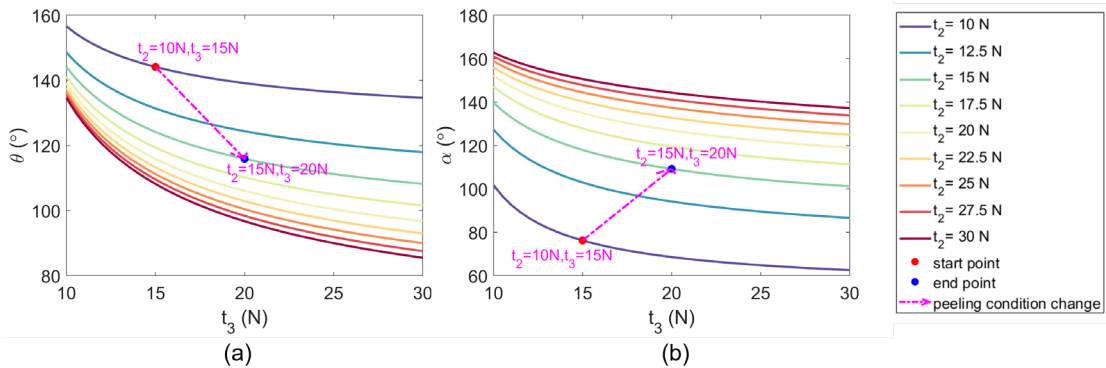
where  $v_i$  is the rewinding roller velocity. The roller dynamics can be described as [18]

$$\dot{v}_i = -\frac{f_i}{J_i} \cdot v_i - \frac{R_i^2}{J_i} \cdot t_i + \frac{R_i}{J_i} \cdot u_i, \quad i = 2, 3 \quad (8)$$

Around an equilibrium operating point, the tension and roller dynamics in (7) and (8) can be described as

$$\Delta \dot{t}_i = K_i \cdot \Delta v_i \quad (9)$$

$$\Delta \dot{v}_i = -\frac{f_i}{J_i} \cdot \Delta v_i - \frac{R_i^2}{J_i} \cdot \Delta t_i + \frac{R_i}{J_i} \cdot \Delta u_i \quad (10)$$


 Figure 7: Steady-state analysis: (a)  $\theta$  map (b)  $\alpha$  map

The transfer function from the input torque variation to the tension variation can be expressed as

$$\frac{\Delta T_i(s)}{\Delta U_i(s)} = \frac{K_i R_i}{J_i s^2 + f_i s + K_i R^2} \quad (11)$$

### 3.2 Peeling Tension Control

As shown in Eqn. (11) the tension-torque variation dynamics can be approximated as a second-order system. A PI controller  $C_i(s)$  can be designed to track the peeling tensions as

$$C_i(s) = K_{P_i} + \frac{K_{I_i}}{s} \quad (12)$$

The closed loop transfer function can be written as

$$G_{cl_i}(s) = \frac{K_i K_{P_i} R \cdot s + K_i K_{I_i} R}{J_i s^3 + f_i s^2 + (K_i R^2 + K_i K_{P_i} R) \cdot s + K_i K_{I_i} R} \quad (13)$$

In order to improve the tension tracking performance, a ZPETC scheme is proposed. The idea of the control design is to cancel the closed-loop poles and cancellable zeros so that the overall transfer function of the system is 1. The control diagram is shown in Fig. 8.  $P_i(s)$  is the plant describing the tension dynamics. The transfer function of the feedforward block  $F_i(s)$  is given as

$$F_i(s) = \frac{J_i s^3 + f_i s^2 + (K_i R^2 + K_i K_{P_i} R) \cdot s + K_i K_{I_i} R}{(\tau s + 1)^2 (K_i K_{P_i} R \cdot s + K_i K_{I_i} R)} \quad (14)$$

It can be seen that the closed-loop transfer function is inverted in  $F_i(s)$ . However, the inverse of the closed-loop transfer function is physically unrealizable because the order of the numerator is 2 orders higher than the denominator. To make the feedforward controller realizable, a filter with the form of  $\frac{1}{(\tau s + 1)^2}$  is added. The high frequency noise amplification could also be limited with the filter.

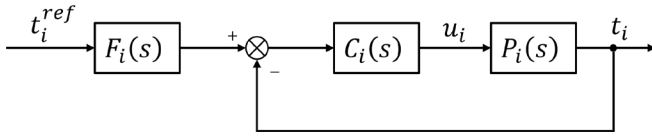


Figure 8: Control block diagram

### 3.3 Tension Control Simulation

The proposed tension control scheme is tested on the R2R peeling simulation model developed in our previous study [17]. Tension controllers that control the peeling tensions on both sides are designed and simulated. The simulation is performed in MATLAB/Simulink environment. The parameters used for the simulation is shown in Table 1. The parameters are obtained based on the experimental setup shown in Fig. 1. The adhesion energy of the laminate is set as 45 N/m.

**Table 1. System Parameters [17]**

Parameters	Value
$E_1, E_2, E_3$	2.7 GPa
$R, R_1, R_2, R_3$	0.0381 m
$D_1$	0.49 m
$D_2$	1.02 m
$D_3$	1.59 m
$h_{w2}, h_{w3}$	127 $\mu$ m
$b$	0.1016 m
$J_2, J_3$	0.9511 kg $\cdot$ m <sup>2</sup>
$f_2, f_3$	19.023 N $\cdot$ m $\cdot$ s/rad
$\Gamma$	80 N/m

The simulation result is shown in Fig. 9. The peeling process was first maintained at a setting of  $t_2 = 10$  N and  $t_3 = 15$  N. The peeling tension setpoint for  $t_2$  was changed to 15 N at time=40 s and it is shown that the peeling tension  $t_2$  converged to 15 N. Due to the interaction effect,  $t_3$  dropped as  $t_2$  rose. It shows that change of peeling tension on one side causes crosstalk effect on the other side. This can be explained by Eqs. (1-6) where the tensions are coupled at the peeling front. The simulation demonstrates that the peeling tensions can be actively tracked by the control scheme.

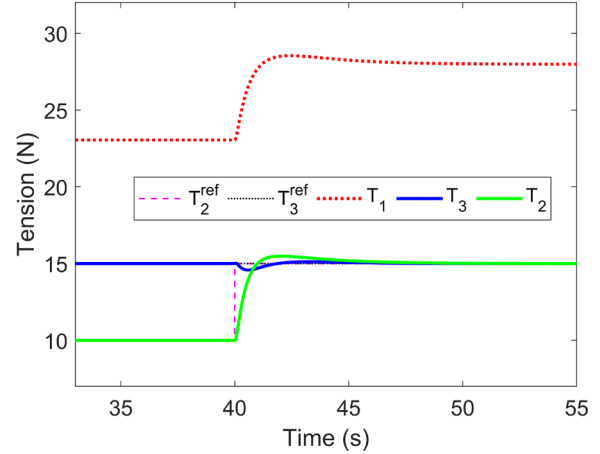


Figure 9: Simulation result

## 4. EXPERIMENTAL RESULTS

Experimental peeling test was conducted to test the functionality of the R2R system and the control scheme. The sample used for the peeling test is prepared by laminating two PET/EVA films using a hot roll laminator. The thickness of the film is 0.005 inches and the width is 4 inches. The experimental result is shown in Fig. 10. The unwinding velocity is set as 0.0045 m/s and the peeling tension setpoint for  $t_2$  are varied from 10 N to 15 N. The setpoint for  $t_3$  is set as 15 N. It is shown that the reference tensions can be tracked by the peeling tension controllers. Similar transient response as in the simulation case can be seen, demonstrating that the proposed tension controller can achieve acceptable tracking performance. The discrepancy in  $t_1$  between the simulation case and the experimental case is due to the varying nature of the adhesion energy in the real world, whereas the adhesion energy is assumed to be constant throughout the simulation.

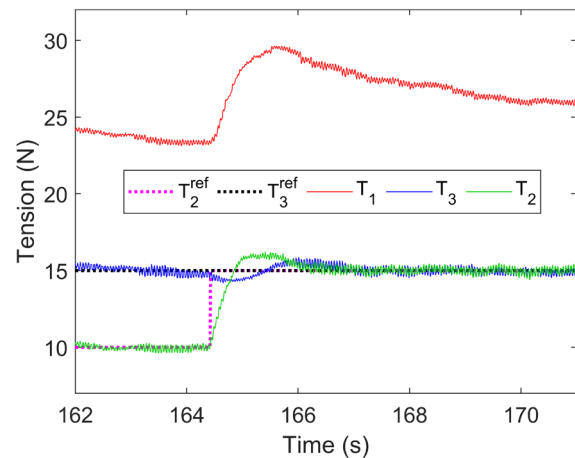


Figure 10: Experimental result

## 5. CONCLUSION

A novel R2R manufacturing system that enables speed and tension controlled mechanical peeling process is

developed. The machine shows the promise of scaling up manufacturing processes, such as dry transfer of 2D materials and transfer printing for flexible electronics. A peeling tension control scheme based on ZPET feedforward and PI feedback control was developed and demonstrated through simulation and experimental data. The developed system has been used to study the tension and speed effect on the quality of the transferred graphene. Future work will include developing control algorithms for peeling angle control, which is expected to have a major impact on the quality of 2D material transfer and transfer printing.

#### ACKNOWLEDGMENTS

This work is based upon work supported primarily by the National Science Foundation under Cooperative Agreement No. EEC-1160494 and CMMI-2041470. Any opinions, findings and conclusions or recommendations expressed in this material are those of the author(s) and do not necessarily reflect the views of the National Science Foundation.

#### REFERENCES

- [1] Kobayashi, T., Bando, M., Kimura, N., Shimizu, K., Kadono, K., Umezumi, N., Miyahara, K., Hayazaki, S., Nagai, S., Mizuguchi, Y. and Murakami, Y., 2013. Production of a 100-m-long high-quality graphene transparent conductive film by roll-to-roll chemical vapor deposition and transfer process. *Applied Physics Letters*, 102(2), p.023112.
- [2] Polsen, E.S., McNerny, D.Q., Viswanath, B., Pattinson, S.W. and Hart, A.J., 2015. High-speed roll-to-roll manufacturing of graphene using a concentric tube CVD reactor. *Scientific reports*, 5(1), pp.1-12.
- [3] Jain, K., Klosner, M.A.R.C., Zemel, M.A.R.C. and Raghunandan, S., 2005. Flexible electronics and displays: high-resolution, roll-to-roll, projection lithography and photoablation processing technologies for high-throughput production. *Proceedings of the IEEE*, 93(8), pp.1500-1510.
- [4] Krebs, F.C., Gevorgyan, S.A. and Alstrup, J., 2009. A roll-to-roll process to flexible polymer solar cells: model studies, manufacture and operational stability studies. *Journal of Materials Chemistry*, 19(30), pp.5442-5451.
- [5] Søndergaard, R., Hösel, M., Angmo, D., Larsen-Olsen, T.T. and Krebs, F.C., 2012. Roll-to-roll fabrication of polymer solar cells. *Materials today*, 15(1-2), pp.36-49.
- [6] Zhang, Y.I., Zhang, L. and Zhou, C., 2013. Review of chemical vapor deposition of graphene and related applications. *Accounts of chemical research*, 46(10), pp.2329-2339.
- [7] Zhao, Q., Hong, N., Chen, D. and Li, W., 2020, September. Controlling Peeling Front Geometry in a Roll-to-Roll Thin Film Transfer Process. In *International Manufacturing Science and Engineering Conference (Vol. 84256, p. V001T05A017)*. American Society of Mechanical Engineers.
- [8] Xin, H., Zhao, Q., Chen, D. and Li, W., 2018. Roll-to-roll mechanical peeling for dry transfer of chemical vapor deposition graphene. *Journal of Micro and Nano-Manufacturing*, 6(3).
- [9] Huang, Y., Liu, H., Xu, Z., Chen, J. and Yin, Z., 2018. Conformal peeling of device-on-substrate system in flexible electronic assembly. *IEEE Transactions on Components, Packaging and Manufacturing Technology*, 8(8), pp.1496-1506.
- [10] Hong, N., Kireev, D., Zhao, Q., Chen, D., Akinwande, D. and Li, W., Roll-to-Roll Dry Transfer of Large-Scale Graphene. *Adv. Mater.* 2021, 2106615, doi: 10.1002/adma.202106615.
- [11] Qin, Z., Xu, Z. and Buehler, M.J., 2015. Peeling silicene from model silver substrates in molecular dynamics simulations. *Journal of Applied Mechanics*, 82(10), p.101003.
- [12] Linghu, C., Zhang, S., Wang, C. and Song, J., 2018. Transfer printing techniques for flexible and stretchable inorganic electronics. *npj Flexible Electronics*, 2(1), pp.1-14.
- [13] Zhou, H., Qin, W., Yu, Q., Cheng, H., Yu, X. and Wu, H., 2019. Transfer printing and its applications in flexible electronic devices. *Nanomaterials*, 9(2), p.283.
- [14] Yoo, B., Cho, S., Seo, S. and Lee, J., 2014. Elastomeric angled microflaps with reversible adhesion for transfer-printing semiconductor membranes onto dry surfaces. *ACS applied materials & interfaces*, 6(21), pp.19247-19253.
- [15] Ghazali, R., Sam, Y.M., Rahmat, M.F.A. and Hashim, A.W.I.M., 2012. Simulation and experimental studies on perfect tracking optimal control of an electrohydraulic actuator system. *Journal of Control Science and Engineering*, 2012.
- [16] Liu, L., Tian, S., Xue, D., Zhang, T. and Chen, Y., 2019. Industrial feedforward control technology: a review. *Journal of Intelligent Manufacturing*, 30(8), pp.2819-2833.
- [17] Zhao, Q., Hong, N., Chen, D. and Li, W., 2021. A Dynamic System Model for Roll-to-Roll Dry Transfer of Two-Dimensional Materials and Printed Electronics. Submitted
- [18] Pagilla, P.R., Siraskar, N.B. and Dwivedula, R.V., 2006. Decentralized control of web processing lines. *IEEE Transactions on control systems technology*, 15(1), pp.106-117.